

Collective surface modes in a fractal cluster of spheres

F. Claro

Facultad de Física, Pontificia Universidad Católica de Chile, Casilla 306, Santiago 22, Chile

R. Fuchs

Ames Laboratory and Department of Physics and Astronomy, Iowa State University, Ames, Iowa 50011

(Received 21 January 1991)

We present a theory for finding the collective surface modes in the quasistatic approximation for a fractal cluster of spheres constructed in a recursive manner. The surface-mode positions and strengths are given in terms of the spectral representation for the polarizability of the cluster. Calculations using the dipole approximation for a cluster constructed recursively from an octahedral arrangement of six spheres show that the surface-mode spectrum is approximately self-similar. We calculate the distribution of scaling indices, $f(\alpha)$, for this spectrum as a function of the fractal dimension of the cluster in Euclidean space.

I. INTRODUCTION

It has been known for several years that random aggregates of particles formed by irreversible processes have fractal character,^{1,2} and there have been many studies of the optical properties of such aggregates. The fractal dimension of these systems can be determined from the static structure factor $S(q)$, which can be found by light-scattering experiments.³ Using computer-generated aggregates of spherical particles, $S(q)$ can be calculated.^{4,5} In order to take account of the interaction between very near or touching spheres, high multipoles must be included; this is the most difficult part of the calculation.

There have also been many experimental and theoretical investigations of optical absorption by aggregates; a recent review is given by Kreibig, Quinten, and Schönauer.⁶ If the particles are metallic spheres, the single absorption peak (Mie resonance) that occurs for isolated spheres is broadened when the spheres form aggregates, and often a pair of absorption peaks is seen; also, the far-infrared absorption is many orders of magnitude larger than for isolated spheres.

In order to take account of the geometrical structure of the aggregate, one must go beyond the simplest mean-field theories (the Maxwell-Garnett theory and the Bruggeman effective-medium theory). For aggregates containing two to ten spheres direct calculations of absorption (in the quasistatic approximation) and both absorption and extinction (when retardation is included) are possible.⁶⁻¹⁰ If the aggregates contain a large number of particles, a variety of theoretical methods have been used, depending on the structure of the aggregate. The fractal character of aggregates has been considered in theories using a differential effective-medium theory,¹¹ renormalization-group methods,^{12,13} random resistor network models,¹⁴ an effective-medium theory with a position-dependent filling fraction,¹⁵ and a statistical model with a pair distribution appropriate for a fractal.¹⁶ If the aggregates form continuous networks extending throughout space, the system can pass through a percolation thresh-

old, and scaling theories can be applied.¹⁷⁻¹⁹ For more dense random aggregates filling all space, models consisting of disordered arrangements of particles on a lattice have been used.^{20,21}

In this paper we study optical absorption by deterministic, recursively constructed three-dimensional fractal aggregates of spherical particles. Experimental and theoretical studies of light scattering by one- and two-dimensional fractal structures (Cantor bars and Vicsek fractals) show that the structure factor $S(q)$ has approximately self-similar properties.²² As one proceeds in the recursive construction of the fractal, the peaks in $S(q)$ split repeatedly, and many groups of narrower peaks appear, with each group having a structure similar to that of the original group.

In our calculations, we use a spectral representation, which gives the depolarization factors and strengths of surface modes, which are related directly to optical absorption peaks if the spheres are metallic. Whereas the peaks in $S(q)$ always have a finite width, the surface modes are discrete at every stage of iteration. The spectrum of depolarization factors is approximately self-similar; in fact, it is a multifractal, and in Sec. III we calculate the distribution of scaling indices $f(\alpha)$.^{23,24} A discussion of the possible experimental relevance of our results is given in Sec. IV.

II. POLARIZABILITY OF A FRACTAL CLUSTER OF SPHERES

In this section we describe the iterative procedure used to determine the polarizability of a fractal collection of spheres in terms of the polarizability of its generator. To illustrate the geometrical construction of the fractal, consider a cluster of $N=4$ spheres in a square, as shown in the left-hand side of Fig. 1(a). This cluster constitutes the generator, and is the first stage in our construction. In the second stage, four of these generators are used as units to construct a geometrically similar but larger square, containing in total $N^2=16$ spheres. Each gen-

erating unit is shown in the right-hand side of Fig. 1(a) as a dashed sphere. The process is repeated recursively, so that at stage j there are N^j spheres in the planar set. Similarly, one can construct a three-dimensional fractal starting with a three-dimensional cluster of spheres as a generator. Figures 1(b) and 1(c) show examples of such generators exhibiting octahedral symmetry, with $N=6$ and $N=7$ spheres, respectively. In this paper we treat the $N=6$ case because it allows us to go to higher filling fractions.

The dielectric response of the structure is strongly influenced by the interaction between the spheres, and an exact solution is difficult to obtain. A convenient approach is to calculate the polarizability of the structure iteratively. This is possible if we assume at each stage that the structure used as a unit for the next stage is replaced by an equivalent sphere with the same polarizability. The approximation works best if the generating cluster of spheres is a highly symmetric arrangement, as is the one we treat in this work [Fig. 1(b)]. There is still some ambiguity in the size of the equivalent sphere. We choose its radius so that, if neighboring spheres in the generator touch each other (and the equivalent spheres also touch each other), the spheres in a given generator touch the spheres in neighboring generators as well. Therefore the percolation threshold for spheres in the generator corresponds to the percolation threshold throughout the entire fractal structure. For example, in the octahedral cluster with $N=6$ spheres shown in Fig. 1(b) with sphere radius a and distance $R=2a\sigma$ between nearest neighbors, the radius of the equivalent sphere (shown by the dashed circle) is $a^{(1)}=\frac{1}{2}R+a=a(1+\sigma)$. For an octahedral cluster with $N=7$ spheres shown in Fig. 1(c), where there is a sphere at the center, the same criterion gives $a^{(1)}=a(1+\sqrt{2}\sigma)$. The validity of this choice of radius can be tested only by more accurate calculations using the actual arrangements of physical spheres in the fractal structure.

Throughout this entire procedure, we will use the dipole approximation; that is, we neglect the higher multipoles, which should be used to calculate the polarizability of a sphere cluster. From accurate calculations for systems of spheres, it is known that the dipole approximation is reasonably accurate if a separation parameter $\sigma=2a/R \geq 1.2$, where a is the sphere radius and R is the distance between sphere centers.⁹

One basic equation needed is that for the polarizability of a sphere of volume v , composed of a dielectric material ϵ :

$$\alpha_{\text{sph}} = v \langle \chi \rangle_{\text{sph}}, \quad (2.1)$$

where

$$4\pi \langle \chi \rangle_{\text{sph}} = [(4\pi\chi)^{-1} + \frac{1}{3}]^{-1}, \quad (2.2)$$

with $\chi = (\epsilon - 1)/4\pi$ the susceptibility of the sphere material. Equations (2.1) and (2.2) are equivalent to the more commonly used expression $\alpha_{\text{sph}} = a^3(\epsilon - 1)/(\epsilon + 2)$. We also use the spectral representation for the polarizability of the spheres in the generator, with total volume Nv :

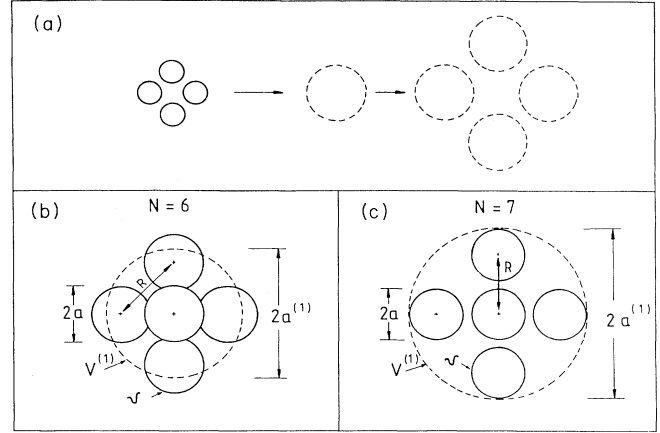


FIG. 1. (a) A cluster of spheres (the generator) is replaced by a single equivalent sphere, which is used to construct a larger cluster in a self-similar manner. The procedure is repeated recursively. (b) Geometry of an octahedral cluster with $N=6$ spheres (no sphere at the center). Each sphere has diameter $2a$ and volume v , and the distance between the centers of nearest-neighbor spheres is R . The equivalent sphere, with diameter $2a^{(1)}$ and volume $V^{(1)}$, is shown by a dashed curve. (c) Geometry of an octahedral cluster with $N=7$ (spheres at center).

$$\alpha^{(1)} = Nv \frac{1}{4\pi} \sum_s \frac{C_s}{(4\pi\chi)^{-1} + n_s}, \quad (2.3)$$

where C_s and n_s are, respectively, the dipole strengths and depolarization factors for the collective surface modes, quantities that depend only on the geometrical arrangement of spheres in the generator. In writing Eq. (2.3) we have assumed that the generator has cubic symmetry, so its polarizability $\alpha^{(1)}$ is a scalar. The total strength of the modes is $\sum_s C_s = 1$, and the modes have a center of $\frac{1}{3}$: $\sum_s C_s n_s = \frac{1}{3}$, and they lie in the range $0 < n_s < 1$. In the following development we shall introduce new "mode positions" $y_s = n_s - \frac{1}{3}$, which are convenient because their centroid is zero: $\sum_s C_s y_s = 0$.

As shown in Fig. 1(b) we replace the N spheres in the generator by an equivalent single sphere of volume $V^{(1)}$, filled with a material $\chi_e^{(1)}$ chosen so the single sphere has the correct polarizability:

$$\alpha^{(1)} = \alpha_{\text{sph}} = V^{(1)} \frac{1}{4\pi} [(4\pi\chi_e^{(1)})^{-1} + \frac{1}{3}]^{-1} \quad (2.4)$$

or

$$\begin{aligned} (4\pi\chi_e^{(1)})^{-1} + \frac{1}{3} &= \frac{V^{(1)}}{4\pi\alpha^{(1)}} \\ &= \frac{V^{(1)}}{Nv} \left[\sum_s \frac{C_s}{(4\pi\chi)^{-1} + n_s} \right]^{-1}. \end{aligned} \quad (2.5)$$

Introducing the variables

$$y = -[(4\pi\chi)^{-1} + \frac{1}{3}], \quad (2.6a)$$

$$y^{(1)} = [(4\pi\chi_e^{(1)})^{-1} + \frac{1}{3}], \quad (2.6b)$$

and letting $Nv/V^{(1)}=F$, the filling fraction of spheres in the equivalent sphere, Eq. (2.5) can be written

$$y^{(1)} = \left[F \sum_s \frac{C_s}{y - y_s} \right]^{-1}, \quad (2.7)$$

where $y_s = n_s - \frac{1}{3}$.

This procedure is continued iteratively. For example, the polarizability of the cluster at the j th stage, as in Eq. (2.4), is

$$\alpha^{(j)} = V^{(j)} \frac{1}{4\pi} [(4\pi\chi_e^{(j)})^{-1} + \frac{1}{3}]^{-1}. \quad (2.8)$$

This is expressed in terms of the effective susceptibility $\chi_e^{(j-1)}$ of the spheres, which make up the cluster, as in Eq. (2.5):

$$(4\pi\chi_e^{(j)})^{-1} + \frac{1}{3} = \frac{V^{(j)}}{NV^{(j-1)}} \left[\sum_s \frac{C_s}{(4\pi\chi_e^{(j-1)})^{-1} + n_s} \right]^{-1}. \quad (2.9)$$

If we introduce the variables

$$y^{(j)} = -[(4\pi\chi_e^{(j)})^{-1} + \frac{1}{3}], \quad (2.10)$$

and note that $NV^{(j-1)}/V^{(j)}=F$, Eq. (2.9) becomes

$$y^{(j)} = \left[F \sum_s \frac{C_s}{y^{(j-1)} - y_s} \right]^{-1}. \quad (2.11)$$

Equation (2.7) defines $y^{(1)}$ as a function of y : $y^{(1)}=h(y)$. Similarly, Eq. (2.11) defines $y^{(j)}$ as the same function of $y^{(j-1)}$,

$$y^{(j)} = h(y^{(j-1)}). \quad (2.12)$$

Equation (2.12) is a map, which can be used iteratively to find successive variables $y^{(1)}, y^{(2)}, \dots, y^{(j)}$ as a function of y , beginning with $y^{(1)}=h(y)$.

We can now find the collective surface mode spectrum of the final fractal structure at stage (j). Using Eq. (2.10), we can rewrite the polarizability $\alpha^{(j)}$ in Eq. (2.8),

$$\alpha^{(j)} = -\frac{V^{(j)}}{4\pi y^{(j)}}. \quad (2.13)$$

The collective surface mode spectrum of the final structure is defined by the strengths $C_m^{(j)}$ and depolarization factors $n_m^{(j)}$ that appear in the spectral representation for $\alpha^{(j)}$:

$$\begin{aligned} \alpha^{(j)} &= \frac{v^{(j)}}{4\pi} \sum_m \frac{C_m^{(j)}}{(4\pi\chi)^{-1} + n_m^{(j)}} \\ &= \frac{v^{(j)}}{4\pi} \sum_m \frac{C_m^{(j)}}{y - y_m^{(j)}}, \end{aligned} \quad (2.14)$$

where $y_m^{(j)} = n_m^{(j)} - \frac{1}{3}$. We are using the symbol m as a general label for the modes at any stage of iteration, whereas the symbol s , which was used previously, is a label for the modes of the generator. For example, in the calculations, which will be discussed in Sec. III, the generator will have two modes, and the structure at stage (j) will have 2^j modes, so $s=1,2$ and $m=1,2, \dots, 2^j$. In Eq. (2.14), $v^{(j)}=N^j v$ is the actual volume of the spheres in the final structure. Since

$$V^{(j)} = (N/F)V^{(j-1)} = \dots = (N/F)^j v,$$

we have

$$v^{(j)} = F^j V^{(j)}. \quad (2.15)$$

Combining Eqs. (2.13), (2.14), and (2.15), we get

$$\sum_m \frac{C_m^{(j)}}{y - y_m^{(j)}} = [F^j y^{(j)}]^{-1} = L^{(j)}(y), \quad (2.16)$$

where we have used the fact that $[F^j y^{(j)}]^{-1}$ can be expressed explicitly as a function $L^{(j)}(y)$ using the iterated map $y^{(j)}=h(y^{(j-1)})$. The total strength is $\sum_m C_m^{(j)}=1$, and, since the final structure also has cubic symmetry, the centroid sum rule $\sum_m C_m^{(j)} n_m^{(j)} = \frac{1}{3}$ or $\sum_m C_m^{(j)} y_m^{(j)} = 0$ must be satisfied; also one has $0 < n_m^{(j)} < 1$.

The strengths $C_m^{(j)}$ and positions $y_m^{(j)}$ can be determined from Eq. (2.16) by adding a small imaginary quantity $-iw$ to y : $y \rightarrow y - iw$, with $w > 0$, and taking the imaginary part. Each term on the left-hand side of Eq. (2.16) is

$$\begin{aligned} \text{Im} \frac{C_m^{(j)}}{y - y_m^{(j)} - iw} &= C_m^{(j)} \frac{w}{(y - y_m^{(j)})^2 + w^2} \\ &\rightarrow \pi C_m^{(j)} \delta(y - y_m^{(j)}) \text{ as } w \rightarrow 0. \end{aligned} \quad (2.17)$$

Hence, Eq. (2.16) gives

$$\sum_m C_m^{(j)} \delta(y - y_m^{(j)}) = \lim_{w \rightarrow 0} \frac{1}{\pi} \text{Im} L^{(j)}(y - iw). \quad (2.18)$$

In numerical calculations using the above procedure one cannot take the limit $w \rightarrow 0$ but must choose a finite value for w , so that, from Eq. (2.17), each mode (m) is represented by a Lorentzian peak of width w and area $C_m^{(j)}$ centered at $y = y_m^{(j)}$. The left-hand side of Eq. (2.18) is then replaced by a continuous spectral function,

$$g^{(j)}(y) = \frac{1}{\pi} \text{Im} L^{(j)}(y - iw), \quad (2.19)$$

with total area $\int g^{(j)}(y) dy = 1$. The spectral function $G^{(j)}(n)$, a function of the depolarization factor variable $n = \frac{1}{3} + y$, is $G^{(j)}(n) = g^{(j)}(n - \frac{1}{3})$.

To illustrate the procedure discussed above, we have calculated the surface mode spectrum for a fractal structure constructed from an octahedral generator of six spheres as shown in Fig. 1(b). We shall consider modes in which the total dipole moment of the octahedron of spheres lies along a symmetry axis, which we will denote as the z axis. There are, of course, degenerate modes with dipole moments in the x , y , and z directions. In the dipole approximation, the generator has two modes, with strengths $C_1=0.69754$ and $C_2=0.30246$, which are independent of the distance between spheres, and with positions $y_1 = -0.05252/\sigma^3$, $y_2 = 0.12112/\sigma^3$, where $\sigma = R/2a$. These results were found using the procedure discussed in Ref. 25. In mode 1, the dipoles on all six spheres are parallel, and in mode 2 the dipoles on the two spheres along the z axis are antiparallel to the dipoles on the four spheres lying on the plane $z=0$.

We find that at each stage of iteration, the number of modes doubles. The spectral function $G^{(j)}(n)$ calculated

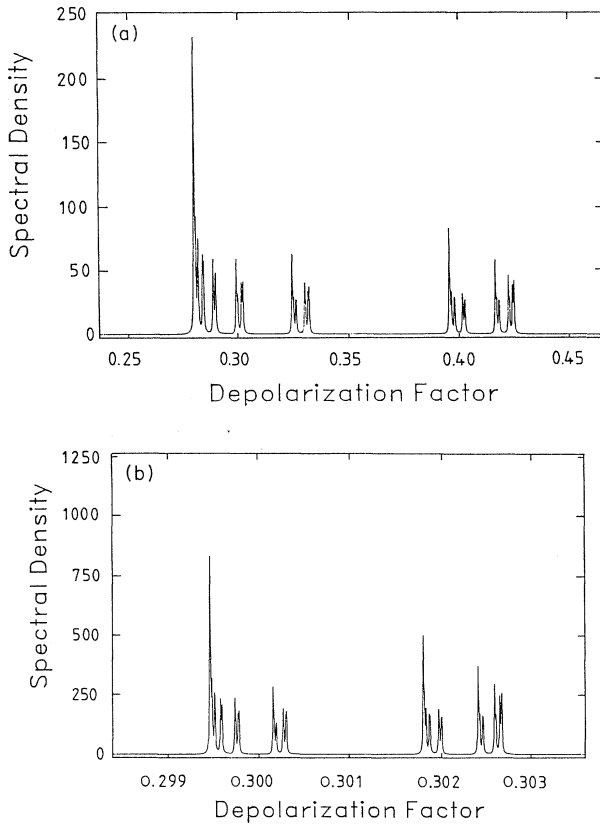


FIG. 2. (a) Spectral density function $G^{(j)}(n)$ for $j=30$ iterations using the $N=6$ octahedral generator with spacing parameter $\sigma=1.2$, and width parameter $w=1.7 \times 10^{-4}$. (b) A small part of the spectral density function centered at $n \sim 0.30$ is shown on an expanded scale, with a width parameter $w=4.5 \times 10^{-6}$.

from Eq. (2.19) for $j=30$ iterations, with a spacing parameter $\sigma=1.2$, is shown in Fig. 2(a). Since there are 2^{30} modes, they cannot be resolved; however, a width parameter $w=1.7 \times 10^{-4}$ allows some of the fine structure to be seen. The spectral function is approximately self-similar. The structure in $G^{(j)}(n)$ centered at about $n=0.30$, in which four peaks are visible in Fig. 2(a), is shown on a magnified scale in Fig. 2(b). One sees a structure that resembles the original complete structure, and, with many repeated magnifications, a similar structure would always reappear.

III. FRACTAL PROPERTIES OF THE SURFACE-MODE SPECTRUM

The surface-mode spectrum is a multifractal set. To understand its properties, we first present in Sec. III A a simple geometrical construction for locating the positions of the modes. In Sec. III B we show how the positions of “bars,” regions in which modes must lie, and “gaps,” regions from which modes are excluded, can be located, and give analogies with the classical Cantor set. Finally, in Sec. III C, we calculate $f(\alpha)$, the distribution of scaling indices, for the mode spectrum.

A. Positions of surface modes

The surface-mode spectrum of the fractal structure at any stage (j) of iteration is determined completely by the function

$$h(y) = \left[F \sum_s \frac{C_s}{y - y_s} \right]^{-1}, \quad (3.1)$$

which depends on the surface-mode spectrum of the generator, and which is used recursively in Eq. (2.12). For convenience, we shall introduce the notation $h^{(j)}(y)$ to denote the function $h(y)$, which has been iterated (j) times. That is, $h^{(1)}(y) \equiv h(y)$, $h^{(2)}(y) = h(h(y))$, etc. In general, $h(h^{(j-1)}(y)) = h^{(j)}(y)$, and

$$y^{(j)} = h^{(j)}(y). \quad (3.2)$$

It can be seen from Eq. (2.14) that the polarizability $\alpha^{(j)} \rightarrow \infty$ when $y \rightarrow y_m^{(j)}$, and from Eq. (2.13) that $y^{(j)} \rightarrow 0$ when $\alpha^{(j)} \rightarrow \infty$. Hence, the mode positions $y_m^{(j)}$, where m labels the mode number, correspond to the zeros of $h^{(j)}(y)$:

$$h^{(j)}(y_m^{(j)}) = 0. \quad (3.3)$$

This is also true for stage 1, when we have the generator: From Eq. (3.1), $h(y_s) = 0$.

In Fig. 3, the function $z = h(y)$ has been plotted, for

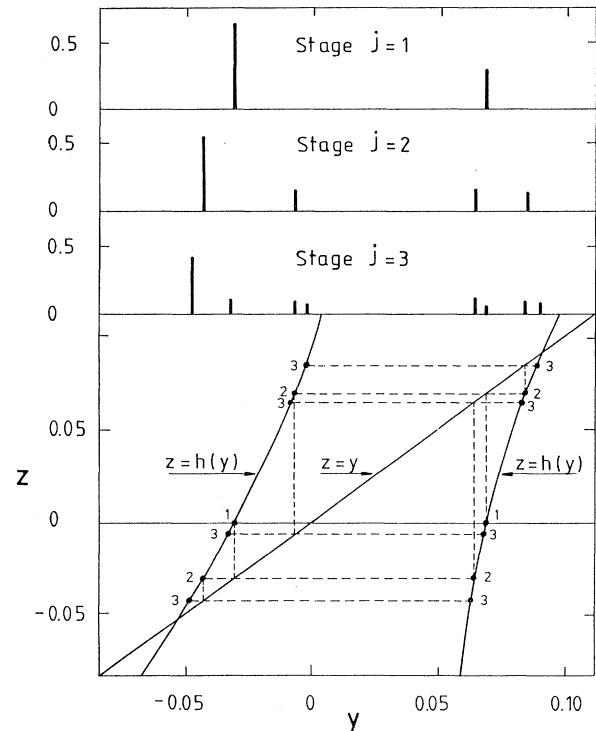


FIG. 3. The functions $z = h(y)$ for the $N=6$ octahedral generator with $\sigma=1.2$, and $z=y$, are shown by solid lines. The dashed lines show the geometrical construction used to locate the positions (y) of the modes for the first three stages of iteration. In the upper part of the figure, the modes are shown for the first three stages, where the height of a line at $y = y_m^{(j)}$ gives the strength $C_m^{(j)}$ of the corresponding mode.

the same octahedral cluster, with $\sigma = 1.2$, which has been used in the calculations leading to Fig. 2. The diagonal line $z = y$, useful for constructing the mode spectrum geometrically, is also shown. The two zeros of $h(y)$, labeled 1, which occur at $y = -0.0304$ and $+0.0701$, are the mode positions y_s of the generator.

The geometrical construction used to find the mode positions for successive stages of iteration is shown by the dashed lines in Fig. 3. From each point labeled 1, a vertical line is drawn until it intersects the line $z = y$. From each point of intersection, a horizontal line is drawn, which intersects the curve $h(y)$ at the points labeled 2. The y values of these four points correspond to the mode positions $y_m^{(2)}$ at the second stage of iteration. A similar construction gives eight points labeled 3, corresponding to the mode positions $y_m^{(3)}$ at the third stage of iteration.

In the upper part of Fig. 3, the modes are shown for the first three stages as vertical lines, with the height of a line at the positions $y_m^{(j)}$ giving the strengths $C_m^{(j)}$ of the modes. The geometrical construction for locating the positions of the modes can be justified as follows. Suppose that $y_m^{(j)}$ is the position of a mode at stage (j) , so that $h^{(j)}(y_m^{(j)}) = 0$ [Eq. (3.3)]. The construction forces $y_m^{(j+1)}$ to satisfy the equation $h(y_m^{(j+1)}) = y_m^{(j)}$. It follows that

$$\begin{aligned} h^{(j+1)}(y_m^{(j+1)}) &\equiv h^{(j)}(h(y_m^{(j+1)})) \\ &= h^{(j)}(y_m^{(j)}) \end{aligned}$$

and therefore, from Eq. (3.3),

$$h^{(j+1)}(y_m^{(j+1)}) = 0. \quad (3.4)$$

Hence, $y_m^{(j+1)}$ is indeed the position of a mode at stage $(j+1)$.

The procedure described above shows only how the mode positions can be found. An algebraic method for finding both the mode positions and amplitudes is described in the Appendix.

B. Bars and gaps in the mode spectrum

In order to analyze the fractal character of the spectral function, it is useful to describe the gaps that appear between modes. The function $h(y)$ has two branches, and, as the number of iterations increases, the modes on each branch approach the fixed points at y_L and y_R (marked f_L and f_R in Fig. 4), where $h(y_f) = y_f$. In general, no modes can exist in regions where $h(y) > y_R$ and $h(y) < y_L$, so there is also a gap between the points labeled 1, at positions y_1 , such that $h(y_1) = y_f$. Thus, from the function $h(y)$ we find two bars in which all modes must lie, and a gap from which they are excluded.

The second iterated function $h^{(2)}(y) = h(h(y))$ has four branches, so there are four bars in which all modes for stages $j \geq 2$ must lie, and three gaps from which they are excluded. One of the gaps is the original one, between the points labeled 1, and two new gaps, between the points labeled 2, appear on each branch. These new gap edges are defined by

$$h^{(2)}(y_2) = h(h(y_1)) = h(y_f) = y_f$$

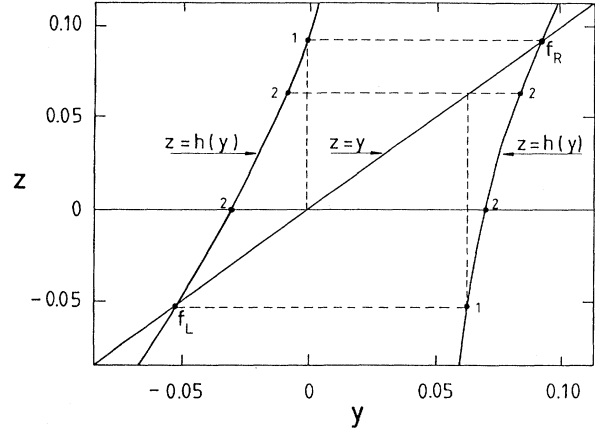


FIG. 4. The same functions $z = h(y)$ and $z = y$ as in Fig. 3. The fixed points f_R and f_L are shown together with dashed lines used to locate the edges of bars and gaps that appear at successive stages of iteration.

so they can be located by the same construction used previously. (The fact that two of the points labeled 2 lie very close to the horizontal axis is coincidental.) Continuing this procedure, from $h^{(3)}(y)$ we find that four new gaps appear, one in each of the previous bars. In general, from $h^{(j)}(y)$ we find $2^j - 1$ gaps, from which the modes obtained for all subsequent iterations $j' \geq j$ are excluded.

This set of bars in which new gaps appear repeatedly is a nonuniform version of the classical Cantor set. Indeed, the classical Cantor set, in which the center third of each bar is removed iteratively, can be obtained using the procedure just described from the function defined by $h(y) = 3y - 2$ and $h(y) = 3y + 2$, for the right-hand and left-hand branches, respectively. The original Cantor bar lies between the fixed points at $y_R = +1$ and $y_L = -1$, and the first gap lies between $y = -\frac{1}{3}$ and $y = +\frac{1}{3}$. At each iteration, a new gap appears in the center third of each bar. In fact, if one introduces "modes" at stage (j) by defining the mode positions $y_m^{(j)}$ from the condition $h^{(j)}(y_m^{(j)}) = 0$, one finds that each of the 2^j bars obtained from $h^{(j)}(y)$ has a mode at its midpoint.

C. Distribution of scaling indices, $f(\alpha)$

The iterative system of bars discussed in Sec. III B is needed for calculating the distribution of scaling indices using the procedure described by Halsey *et al.*²⁴ The first step in the calculation is to divide the fractal set into pieces, in which piece (i) has a measure p_i and lies within a region of size l_i , and to calculate

$$\Gamma(q, \tau) = \sum_{i=1}^n \frac{p_i^q}{l_i^\tau}. \quad (3.5)$$

Applying this equation to our mode spectrum, n is the number of bars in which the modes must lie, $l_i = (\Delta y)_i / (y_R - y_L)$ is the ratio of the width $(\Delta y)_i$ of the i th bar to the overall width of the spectrum, and p_i is the total strength of all modes lying in the i th bar. From the sum rule $\sum_m C_m^{(j)} = 1$, it follows that $\sum_i p_i = 1$, which is a

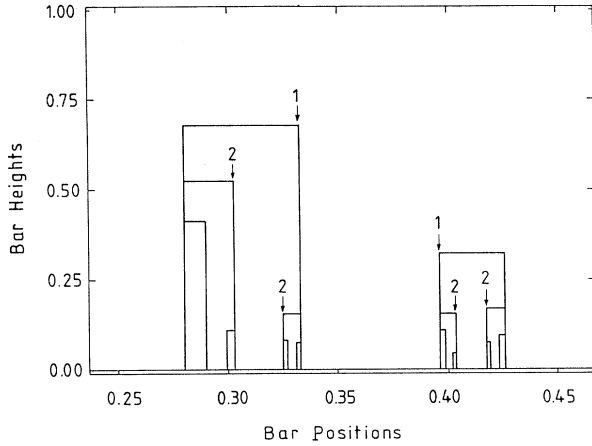


FIG. 5. Bar positions and heights, which appear at the first three stages of iteration. The depolarization factor n is used as the variable on the abscissa.

necessary requirement.

Figure 5 shows sets of 2, 4, and 8 bars obtained from $h^{(1)}(y)$, $h^{(2)}(y)$, and $h^{(3)}(y)$, respectively. The edges of the gaps, which appear at stages (1) and (2), are marked by numbers 1 and 2, which correspond to the numbered points in Fig. 4. The height of a bar is p_i , the total strength of all modes lying in the bar. To continue with the calculation of $f(\alpha)$, one sets $\Gamma(q, \tau) = 1$, defining τ as a function of q . For each value of q , one must find $\alpha(q) = d\tau/dq$ and $f(q) = q\alpha(q) - \tau(q)$. As q varies from a large negative value (-100) to a large positive value ($+100$) the complete functional relation $f(\alpha)$ is determined. Furthermore, the procedure gives generalized dimensions $D_q = \tau(q - 1)$ as a function of q . D_0 is defined as the Hausdorff dimension, $D_{-\infty} = \alpha_{\max}$, and $D_{\infty} = \alpha_{\min}$, where α_{\max} and α_{\min} are, respectively, the upper and lower limits of α in $f(\alpha)$.

Most of the calculations of $f(\alpha)$ were done with $n = 32$ bars and eight iterations, giving $2^8 = 256$ modes, with eight modes lying in each bar. In principle, one should go to a very large number of iterations, since there is some transfer of weight from one bar to another as the iterations proceed. However, calculations with 128 bars and ten iterations show that the above procedure is sufficiently accurate.

The function $f(\alpha)$ for the mode spectrum found with $\sigma = 1.2$ is shown in Fig. 6. This spectrum has a Hausdorff dimension $D_0 = 0.5322$, $\alpha_{\max} = D_{-\infty} = 0.647$, and $\alpha_{\min} = D_{\infty} = 0.311$. To understand the origin of $f(\alpha)$, we can divide the spectrum into n bars and associate a scaling index $\alpha_i = \ln p_i / \ln l_i$ with the i th bar. If we go to the $n \rightarrow \infty$ limit, and the α_i become continuous, $f(\alpha)$ is proportional to the logarithm of the number of times that a given value of α occurs. For each bar, α_i lies in the range $\alpha_{\min} \leq \alpha_i \leq \alpha_{\max}$, where the value $\alpha_i = \alpha_{\min}$ occurs for the bar at the left edge of the spectrum, and the value $\alpha_i = \alpha_{\max}$ occurs for the eleventh bar from the right. Moreover, many more large values than small values of α_i occur; this accounts for asymmetry in $f(\alpha)$. In the nonuniform Cantor sets discussed by Halsey *et al.*,²⁴ α_{\min}

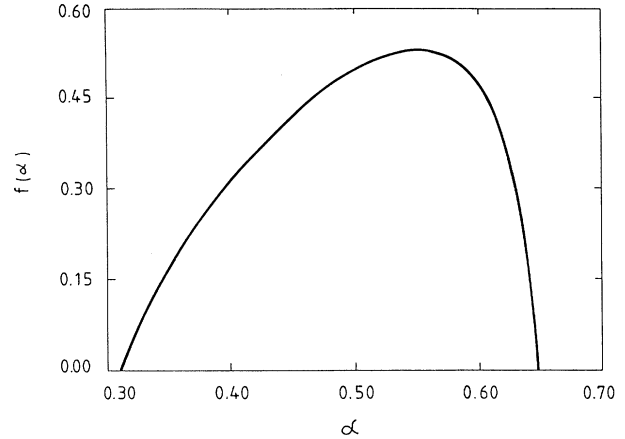


FIG. 6. Distribution of scaling indices $f(\alpha)$, for the surface-mode spectrum shown in Fig. 2.

and α_{\max} are associated with the extreme edges of the set, and this is also true for our surface-mode spectrum for greater distances between spheres ($\sigma > 1.8$), when α_{\max} occurs for the bar at the right edge of the spectrum. The unusual location of α_{\max} for $\sigma < 1.8$ is a consequence of the curvature of the function $h(y)$, which becomes more pronounced as σ decreases.

We also have found the surface-mode spectrum for other values of the sphere separation parameter σ . Since the dipole approximation becomes inaccurate for $\sigma < 1.2$, we consider only $\sigma \geq 1.2$. The most important effect of increasing σ is simply that the two surface modes moves closer together, approaching the centroid $n = \frac{1}{3}$ (or $y = 0$) as $\sigma \rightarrow \infty$. In addition, all scaling indices decrease, approaching zero as $\sigma \rightarrow \infty$. This causes the surface-mode spectrum to have an increasingly "thin" appearance. In the spectrum for $\sigma = 1.2$ shown in Figs. 2(a) and 2(b)

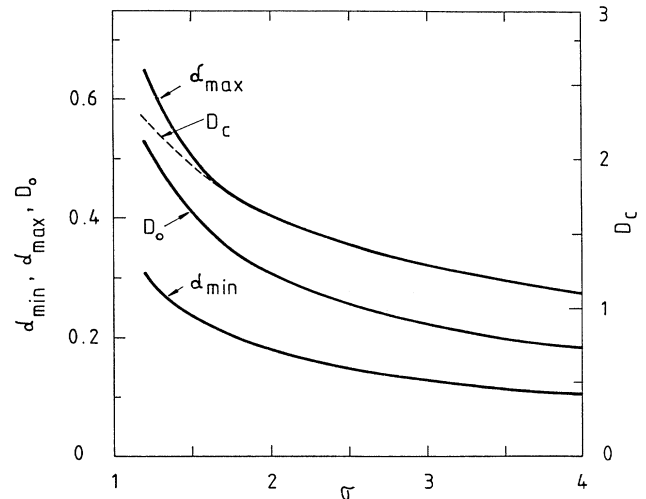


FIG. 7. Maximum and minimum values of the scaling index, and Hausdorff dimension D_0 for the mode spectrum (left-hand scale) and fractal dimension D_c of the recursively constructed cluster (right-hand scale), as functions of the spacing parameter σ .

about 32 modes associated with five stages of iteration are visible at a given magnification. As σ increases, fewer and fewer peaks can be seen, until for $\sigma \geq 10$, only two peaks are visible in any figure. This means, for example, that if one looks at the two peaks associated with the two modes for the generator at the first stage of iteration, a figure at the same scale will still only show two peaks no matter how many iterations are carried out, since the modes contained in each peak cannot be resolved.

Figure 7 gives a plot of the limits α_{\min} and α_{\max} of the scaling indices, and the Hausdorff dimension D_0 , as a function of the separation parameter σ . Also, the fractal dimension D_c of the iterated sphere system in Euclidean space is shown. From the length ratio $(1+\sigma)$ and the mass ratio of six for successive iterations it follows that $D_c = \ln(6)/\ln(1+\sigma)$. One has the result $D_c \approx 4\alpha_{\max}$ if $\sigma \geq 1.7$; however, we do not know if this coincidence has any significance.

IV. DISCUSSION

We have shown how a geometrical structure that has recursive properties exhibits recursive properties in its dielectric response. This follows from the fact that the spectral density of an aggregate, the quantity that characterizes this response, depends only on the geometry.

Our results also show that the response of the system is strongly dependent on the filling fraction of the generator. One can imagine plotting the spectral density using different "magnifications" as in Figs. 2(a) and 2(b), adjusting the width parameter w to be a fixed fraction (say, $\sim 10^{-3}$) of the range in depolarization factor. As the filling fraction decreases (or σ increases), the spectrum has an increasingly sparse appearance; that is, fewer peaks can be seen in a given plot. For sufficiently small filling fractions, only two peaks are seen at a given "magnification." In this case at the first magnification stage only the two peaks inherent to the generator would be visible. If the sphere separation parameter moves into the range $\sigma < 1.2$, the dipole approximation becomes inaccurate, and higher multipoles must be used to describe the interaction between spheres. In this region, the surface mode spectrum of the generator will extend over a broader range and will have more than two peaks. Moreover, there will be wider additional splitting when the fractal structure is built up, so that the spectrum will have a "dense" appearance, with a very large number of peaks visible in a plot of the spectral density function. As one approaches the percolation threshold ($\sigma \rightarrow 1$), one can expect the small-depolarization-factor part of the surface mode spectrum of the fractal structure to depend strongly on its fractal character; indeed, it may have scaling properties similar to that of the low-frequency vibrational spectrum in fractal structures.^{26,27} The strong role that the peak structure of the generator plays in the overall response of the fractal has also been found in other work.¹⁶

Each collective surface mode, with depolarization factor $n_m^{(j)}$, is associated with an absorption peak that occurs at a frequency ω such that $\text{Re}[\epsilon(\omega)] \approx 1 - 1/n_m^{(j)}$, where $0 < n_m^{(j)} < 1$. Therefore, the absorption peaks lie in fre-

quency ranges where $\text{Re}[\epsilon(\omega)] < 0$, or, for metallic spheres, $\omega < \omega_p$. However, because of dissipative mechanisms in the material, $\text{Im}[\epsilon(\omega)] > 0$, and the peaks will have finite width. Also, the minimum sphere size is limited by atomic dimensions, and the maximum sphere size should be less than $\sim 100 \text{ \AA}$, otherwise there will be large red shifts, broadening and further structure due to the breakdown of the quasistatic approximation. Therefore, any fractal structure to which our dipolar results would apply must be restricted to two or three recursive stages. For these reasons, in the regime we have covered, it would be difficult to observe more than four or eight peaks in the absorption spectrum. Note also that besides the presence of a peak structure an important effect of building up the fractal is a widening of the absorption range, as is apparent from the top of Fig. 3 if one attaches a width to the spectral lines. This is a general feature also expected for a disordered cluster¹¹ and is accompanied by an important low-frequency enhancement with respect to the Mie absorption of an isolated sphere.⁴

APPENDIX

In order to calculate the strengths of the modes we proceed as follows. From Eqs. (2.11) and (2.13) one obtains

$$\alpha^{(j)} = -\frac{FV^{(j)}}{4\pi} \sum_s \frac{C_s}{y^{(j-1)} - y_s}.$$

This expression gives the polarizability of a cluster of spheres with the same geometry as the generator and with total volume $FV^{(j)}$, each sphere being filled with an effective medium having response function $y^{(j-1)}$. The corresponding spectral density, as a function of $y^{(j-1)}$, is

$$g^{(j)}(y^{(j-1)}) = \sum_s C_s \delta(y^{(j-1)} - y_s).$$

To express $g^{(j)}$ in terms of the original response function y , we must solve for the 2^{j-1} roots of the equation $y^{(j-1)}(y) = y_s$. Calling these roots $y_{sk}^{(j)}$, using the identity, obtained from Eq. (2.11),

$$\frac{dy^{(j-1)}}{dy} = F^{j-1} \prod_{r=1}^{j-1} \left[(y^{(r)})^2 \sum_{s'} \frac{C_{s'}}{(y^{(r-1)} - y_{s'})^2} \right],$$

where $y^{(0)} \equiv y$, and the property of δ functions,

$$\delta(y^{(j-1)} - y_s) = \sum_k \frac{\delta(y - y_{sk}^{(j)})}{|dy^{(j-1)}/dy|},$$

one gets

$$g^{(j)}(y) = \frac{1}{F^{j-1}} \sum_s C_s \sum_{k=1}^{2^{j-1}} \frac{\delta(y - y_{sk}^{(j)})}{\prod_{r=1}^{j-1} \left[(y^{(r)})^2 \sum_{s'} C_{s'} / (y^{(r-1)} - y_{s'}) \right]}.$$

The depolarization factors and associated strengths of the modes are therefore given by

$$n_{sk}^{(j)} = y_{sk}^{(j)} + \frac{1}{3},$$

$$C_{sk}^{(j)} = \frac{1}{F^{j-1}} \frac{C_s}{\prod_{r=1}^{j-1} \left[(y^{(r)})^2 \sum_{s'} C_{s'} / (y^{(r-1)} - y_{s'}) \right]_{y=y_{sk}^{(j)}}},$$

where the two indices $s = 1, 2$, and $k = 1, 2, \dots, 2^{j-1}$ are equivalent to a single general mode label $m = 1, 2, \dots, 2^j$.

ACKNOWLEDGMENTS

The Ames Laboratory is operated for the U.S. Department of Energy by Iowa State University under Contract No. W-7405-Eng-82. This investigation was supported by the Director for Energy Research, Office of Basic Energy Sciences, U.S. Department of Energy, by the Fondo Nacional de Investigaciones Científicas y Tecnológicas (Grant No. 90/0375) and by the Consejo de Investigación Científica y Tecnológica de Chile.

¹T. A. Witten and L. M. Sander, *Phys. Rev. B* **27**, 5686 (1983).

²L. M. Sander, *Nature (London)* **322**, 789 (1986).

³D. A. Weitz, J. S. Huang, M. Y. Lin, and J. Sung, *Phys. Rev. Lett.* **54**, 1416 (1985).

⁴M. V. Berry and I. C. Percival, *Pot. Act.* **33**, 577 (1986).

⁵Z. Chen, P. Sheng, D. A. Weitz, M. H. Lindsay, M. Y. Lin, and P. Meakin, *Phys. Rev. B* **37**, 5232 (1988).

⁶U. Kreibitz, M. Quinten, and D. Schönauer, *Physica A* **157**, 238 (1989).

⁷P. Clippe, L. Evrard, A. Lucas, and M. Ausloos, *Phys. Rev. B* **18**, 7176 (1978).

⁸J. Gerardy and M. Ausloos, *Phys. Rev. B* **27**, 6446 (1983).

⁹F. Claro, *Phys. Rev. B* **30**, 4989 (1984); **35**, 406 (1987).

¹⁰R. Rojas and F. Claro, *Phys. Rev. B* **34**, 3730 (1986).

¹¹P. M. Hui and D. Stroud, *Phys. Rev. B* **33**, 2163 (1986).

¹²W. A. Curtin and N. W. Ashcroft, *Phys. Rev. B* **31**, 3287 (1985).

¹³S. Berthier and K. Driss-Khodja, *Physica A* **157**, 356 (1989).

¹⁴E. L. Wright, *Astrophys. J.* **320**, 818 (1987).

¹⁵R. Fuchs, *Phys. Rev. B* **35**, 7700 (1987).

¹⁶V. M. Shalaev and M. I. Stockman, *Z. Phys. D* **10**, 71 (1988).

¹⁷K. Ghosh and R. Fuchs, *Phys. Rev. B* **38**, 5222 (1988).

¹⁸F. Brouers, *Physica A* **157**, 454 (1989).

¹⁹Th. Robin and B. Souillard, *Physica A* **157**, 285 (1989).

²⁰A. Liebsch and B. Persson, *J. Phys. C* **16**, 5375 (1983).

²¹P. Sheng, *Physica A* **157**, 238 (1989).

²²C. Allain and M. Cloitre, *Phys. Rev. B* **33**, 3566 (1986); *Phys. Rev. A* **36**, 5751 (1987); *Physica A* **157**, 352 (1989).

²³A. Coniglio, in *Fractals in Physics*, Proceedings of the Sixth Trieste International Symposium, edited by L. Pietronero and E. Tosatti (North-Holland, Amsterdam, 1986), p. 165.

²⁴T. C. Halsey, M. H. Jensen, L. P. Kadanoff, I. Procaccia, and B. I. Shraiman, *Phys. Rev. A* **33**, 1141 (1986).

²⁵R. Fuchs and F. Claro, *Phys. Rev. B* **39**, 3875 (1989).

²⁶S. Alexander and R. Orbach, *J. Phys. (Paris) Lett.* **43**, L625 (1982).

²⁷A. Aharony, S. Alexander, O. Entin-Wohlman, and R. Orbach, *Phys. Rev. B* **31**, 2565 (1985).